A Novel Stochastic Unscented Transform for Probabilistic Drag Modeling and Conjunction Assessment

Rachit Bhatia, Gerardo Josue Rivera Santos
West Virginia University

Jacob D. Griesbach
ARKA/Stratagem

Piyush M. Mehta
West Virginia University

ABSTRACT

Space safety and sustainability has recently received formalized recognition in the light of proliferation by large satellite constellations operated by the commercial sector. Enhanced space operations - detection, characterization, and tracking - are critical for safety and sustainability. A large portion of the lethal (non-)trackable debris reside in low Earth orbit (LEO) while the new commercial constellations reside dominantly in the lower LEO (LLEO) regime with significant plans for exploiting very LEO (VLEO) for future missions. With the new LEO population biased toward LLEO and VLEO, operations have become significantly more sensitive to atmospheric drag, modeling of which remains a primary challenge. Under support from the Intelligence Advanced Research Projects Activity (IARPA) Space Debris Identification and Tracking (SINTRA) program and the Office of Space Commerce (OSC), we are developing the next-generation drag modeling framework that accurately characterizes atmospheric density uncertainty due to space weather in a physics- and data-driven approach. This paper introduces one of the elements of the new framework we call stochastic Unscented Transform (SUT), a mathematical formulation designed to capture the joint statistics of probabilistic atmospheric density models and their probabilistic drivers or inputs. We present the mathematical derivation of SUT and its validation with simple numerical examples of linear and non-linear systems and then apply it to the case of drag modeling by incorporating the effects of uncertainty in the solar driver and density models in real-time orbit propagation. Enabled by the generalized nature of the SUT formulation, we also apply it to uncertainty and orbit prediction. This work moves us in the direction of realistic covariance for operations and eventually space safety and sustainability.

1. INTRODUCTION

The need to include reliable uncertainty information for probabilistic atmospheric density models, like CHAMP-ML [1] and its drivers, for example, F10.7, in the context of drag modeling is critical for accurate orbit prediction and safe space operations in low Earth orbit (LEO). The lack of reliable uncertainty information in dynamic modeling for orbit covariance propagation is typically overcome by employing process noise, Q, that is optimized during the orbit determination process and accounts for un-modeled and/or mis-modeled dynamics [2]. The current operational model for atmospheric drag, the High Accuracy Satellite Drag Model (HASDM) [3], uses the JBH09 [4] empirical density model , a JB2008 [5] variant, to perform forecasts. The forecasts use a time-invariant estimate of thermosphere density uncertainty modeled as a simplified function of perigee altitude and solar activity which can be significantly improved for operations. The HASDM system also does not currently account for driver forecast uncertainty. The next-generation drag modeling framework will leverage models that provide reliable physics- and data-driven uncertainty estimates (Figure 1).

The primary sources of uncertainty in the drag acceleration, $\vec{a}_{drag}$, model described in (Figure 1) are the thermosphere mass density, ρ, and the drag coefficient, C_D. Cross-sectional area, A, and satellite mass, m, are typically well known

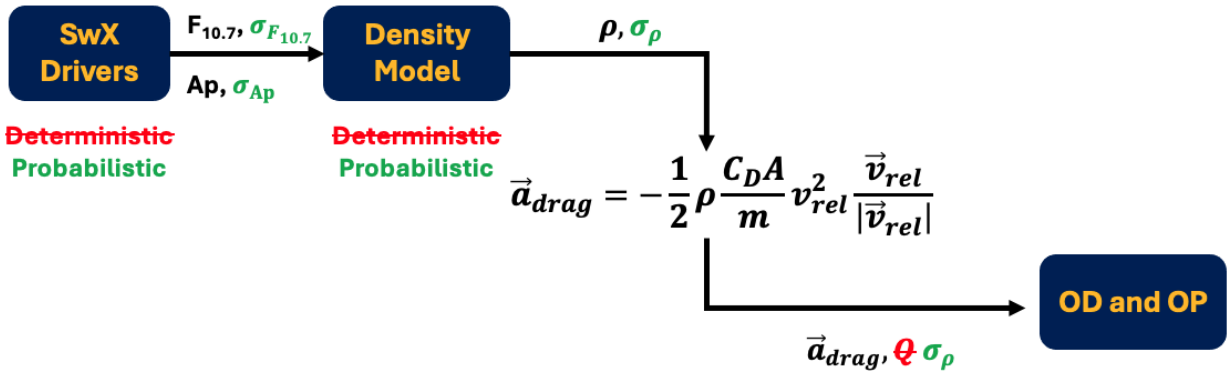

Fig. 1: A schematic of the next-gen drag modeling framework. The elements of the new framework are highlighted in green while those being replaced are strikeout in red. SwX: Space Weather, OD: Orbit Determination, and OP: Orbit Propagation.

but can also be uncertain depending on the object. As a result, they are commonly lumped into a single uncertain ballistic coefficient parameter, $B = \frac{C_D A}{m}$, to simplify the modeling. The final parameter is the velocity of the orbiting object with respect of the co-rotating atmosphere, v_{rel}, which is also generally well known but can induce errors in the presence of strong neutral winds [6]. This work focuses on addressing the uncertainty in ρ.

Despite being climatological with limited fidelity, empirical models such as JB2008/JBH09 and MSIS [7] have been preferred for operations primarily because of the ease-of-use. Physics-based models have been touted as the next big thing for decades, however, the computational cost of such models have kept them from operations. All of the existing models are deterministic. We have recently developed a series of probabilistic empirical and quasi-physical density models (HASDM-ML [8], CHAMP-ML [1], MSIS-UQ [9], and TIE-GCM ROPE [10]). We define probabilistic models as those that provide a stochastic output (density distribution) for a deterministic set of inputs. Additionally, several efforts in the space weather community have led to probabilistic models for space weather (swx) drivers of density models (e.g. F10.7 [11, 12] and Ap/Kp [13, 14]).

Because probabilistic models for orbital dynamics, drag in this case, have only been recently developed, leveraging such capabilities requires a novel mathematical framework to efficiently and effectively capture the joint statistics (driver and model; see Figure 1) for operations. The primary contribution of this work is the development of such a mathematical framework we call Stochastic Unscented Transform (SUT). Unlike the traditional (deterministic) unscented transform (UT) [15], SUT accurately captures the joint statistical characteristics of probabilistic space weather inputs driving stochastic atmospheric density models. This capability enables a more accurate modeling of inherently dynamic systems, providing a more realistic representation of the complex dynamics. Due to the improved state estimation and prediction, this framework can find application across diverse fields, proving particularly beneficial in complex environments where deterministic models fall short, and Monte Carlo simulations become inefficient. Notably, the SUT is well-suited for problems with limited computational resources and is suitable for real-time applications. These attributes make it particularly well-suited for use in space applications. Leveraging this generalization of SUT, as a second contribution, we demonstrate the application of the SUT framework in orbit and uncertainty propagation.

The outline of the paper is as follows: The next section describes in detail the mathematical derivation of the generalized SUT framework. The developed SUT formulation is then validated using simple numerical examples of linear and non-linear systems and then applied to the case of probabilistic density modeling for the drag application (primary contribution). The setup of SUT for orbit and uncertainty propagation (second contribution) and validation with Monte Carlo is presented next. Finally the SUT framework is applied in a 2-tier end-to-end scenario where it is first used to obtain joint uncertainty in density resulting from both driver and model uncertainties and then for real-time orbit and uncertainty/covariance propagation using the estimated joint density uncertainty.

2. SUT DERIVATION

2.1 Problem Statement

The goal of SUT framework is to accurately model the statistical mean and variance for a system using a probabilistic model driven by probabilistic inputs. Any given system can be broadly segmented into three basic components: input, model, and output. Each of these components can be deterministic or probabilistic. While previous studies have investigated systems with probabilistic inputs/outputs, no generic framework exists for incorporating a probabilistic model without linearizing or incorporating some form of approximation.

In the SUT framework, sigma points are defined as a specific set of data points collected from the input distribution. The input can generally have any arbitrary distribution, however, in this work, we consider the input distribution as a best-fit Gaussian distribution. (Similar to a standard unscented transform, the modeling seeks to incorporate and track the first two distribution moments, whether the input distribution is Gaussian or not. Other works investigate capturing higher order moments for cases where it may be needed [16].) Each sigma point includes the effects of uncertainty applied on the input distribution, such that the mean and variance of each sigma point is transformed through the stochastic model to produce new/transformed mean and variance. For N sigma points:

$$\mu_{x_0}, \quad \mu_{x_1}, \quad \ldots, \quad \mu_{x_N} \longrightarrow \begin{Bmatrix} \mu_{y_0} \\ \sigma^2_{y_0} \end{Bmatrix}, \quad \begin{Bmatrix} \mu_{y_1} \\ \sigma^2_{y_1} \end{Bmatrix}, \quad \ldots, \quad \begin{Bmatrix} \mu_{y_N} \\ \sigma^2_{y_N} \end{Bmatrix}$$

where sigma points, $x_0, x_1, x_2, ..., x_N$, smartly sampled from an input distribution, X, are fed through the model to obtain the output points, $y_0, y_1, y_2, ..., y_N$, where each output point is conveyed as a mean and variance, as illustrated in Figure 2. The approach is to treat each sigma point output shown above as best-fit, normally-distributed random variables. Once the input distribution sigma points and weights are defined, these data points are transformed by a probabilistic model to compute output information statistics. These (multiple) sigma-point statistics are then used to compute the overall system transformation distribution, Y, not only incorporating the properties of the input distribution, but also the uncertainties associated with the model transform itself.

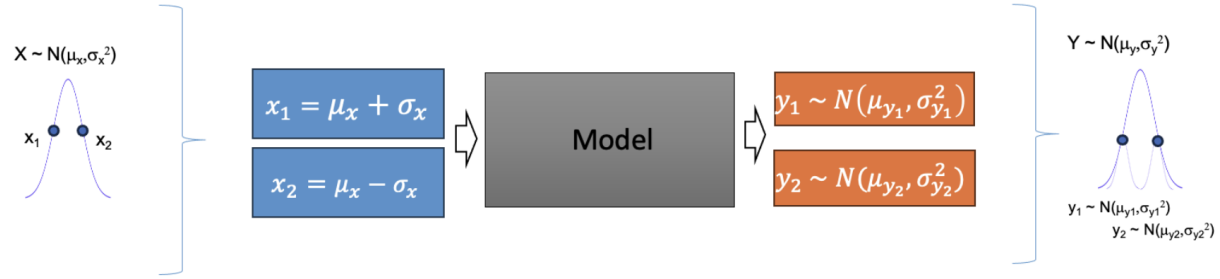

Fig. 2: Schematic Diagram of the SUT framework.

2.2 Standard "Deterministic" Unscented Transform

The common approach known for the Unscented Transform is to track the first and second moments of an input distribution through a (semi-) arbitrary nonlinear function [17]. We call this standard unscented technique "deterministic" because it treats the underlying transformation as a deterministic model; it does not consider any uncertainty from the model/transformation itself. Here, provided an input value, the model provides a (deterministic) output value with no reported uncertainty.

By choosing smartly sampled sigma points along with only attempting to track the first and second order moments, applying an unscented approach is more efficient than Monte Carlo or particle filtering techniques. The principle of this idea stands by selecting specific points known as *sigma points* obtained from the Gaussian input distribution's mean $\tilde{\mu}_x$ and variance $\tilde{\sigma}^2_x$. While the methodology within the paper can address higher-dimensional cases, we only address a single dimension (1D) herein. With this information, the sigma points and a set of weights can be obtained. The input sigma point values are defined as x_i with selected unscented weights for mean estimation, w^a_i, and variance,

w_i^c, estimation. From previous contributions, different algorithms exist to select sigma point locations and weights using a set of scaling parameters [18].

Let the location of the sigma point relative to the mean (in units of standard deviations or σ) be defined as s_i, so that sigma-points are located at $\mu + s_i\sigma$. For example, $s_i = 1$ defines a sigma-point located at $\mu + 1\sigma$, and $s_i = -1$ defines a sigma-point located at $\mu - 1\sigma$. Then weights may be selected arbitrarily as long as they follow

$$\sum_{i=0}^{N} w_i^a s_i = 0 \tag{1}$$

$$\sum_{i=0}^{N} w_i^a = 1 \tag{2}$$

for the mean estimator, and for a valid variance estimator,

$$\sum_{i=0}^{N} w_i^c = 1 \tag{3}$$

$$\text{with } w_i^c = 0 \quad \text{for/if} \quad s_i = 0. \tag{4}$$

Adherence to the above constraints ensure that the sigma points can result in unbiased overall system estimates.

By translating the input sigma point values, x_i, through the (deterministic) model, f, we obtain output values as

$$y_i = f(x_i). \tag{5}$$

where we can estimate the desired statistics of the overall system mean μ_y and variance σ_y^2 as

$$\tilde{\mu}_y = \sum_{i=0}^{N} w_i^a y_i \tag{6}$$

$$\tilde{\sigma}_y^2 = \sum_{i=0}^{N} \frac{w_i^c}{s_i^2} (y_i - \tilde{\mu}_y)^2, \tag{7}$$

where we use a tilde to denote estimated values.

The above equations may be proven by inserting the input sigma points x_i into Equations (6) and (7) and the result would match the mean μ_x and the variance σ_x, respectively.

The investigations developed in this work led us to analyze a case of a common set of $N = 2$ sigma points chosen simply at $\mu \pm \sigma$.

2.2.1 Common Symmetric $N = 2$

Here, sigma points are selected by evenly weighting two data points around the mean. The collection of these points are $x_0 = \mu_x + \sigma_x$ and $x_1 = \mu_x - \sigma_x$. By the nature of the symmetric approach, when the average is taken for both sigma points, we obtain the mean of the input distribution. To preserve this observation, the value for the weights of each point are $w_0^a = w_1^a = w_0^c = w_1^c = \frac{1}{2}$. With this, the mean (6) and covariance (7) can be rewritten as

$$\tilde{\mu}_y = \frac{1}{2}(y_0 + y_1) \tag{8}$$

$$\tilde{\sigma}_y^2 = \frac{1}{4}(y_0 - y_1)^2 \tag{9}$$

We choose this (common symmetric $N = 2$ case) for its simplicity. Other cases may be considered such as asymmetric cases (where $w_i^a \neq w_i^c$) and also cases with additional sigma points.

2.3 Stochastic Unscented Transform

The next step is to evolve the unscented transform to incorporate probabilistic modeling (using the symmetric case). The main characteristic of this method is that we are implementing the same rules as the deterministic unscented transform, but instead of having scalars, we are working with model *output distributions*. Here, model outputs are provided as a mean value with an associated uncertainty variance, $y_i = (\mu_{y_i}, \sigma^2_{y_i})$. Also, importantly, we assume herein that each resultant sigma point distribution is independent.

Considering the deterministic mean and variance estimators, we derive new stochastic mean and variance estimators by carrying through each sigma-point output result as a distribution. Here we denote Y as the overall system output distribution.

2.3.1 General Mean Estimator

Using (6), the resultant mean is the weighted sum of all of the y_i output sigma points. Based on this, we develop a general mean estimator that can be applied to any set of sigma points with their appropriate weights. Since each Y output sigma point represents a normal distribution, the distribution for the weighted sum associated with the mean estimator for Y can be described as

$$\sum_{i=0}^{N} w_i^a \mathcal{N}\left(\mu_{y_i}, \sigma^2_{y_i}\right) \sim \mathcal{N}\left(\sum_{i=0}^{N} w_i^a \mu_{y_i}, \sum_{i=0}^{N} \left(w_i^a\right)^2 \sigma^2_{y_i}\right) \sim \mathcal{N}\left(\tilde{\mu}_y, \tilde{\sigma}^2_{\mu_y}\right), \tag{10}$$

again assuming each sigma point is independently distributed. Thus,

$$\tilde{\mu}_y = \sum_{i=0}^{N} w_i^a \mu_{y_i} \tag{11}$$

$$\tilde{\sigma}^2_{\tilde{\mu}_y} = \sum_{i=0}^{N} \left(w_i^a\right)^2 \sigma^2_{y_i} \tag{12}$$

The weighted sum of (independent) normal distributions remains normal, where weighted means and squared weighted variances add. It is important to note that $\tilde{\sigma}^2_{\tilde{\mu}_y}$ is the estimated variance of the mean estimator, and not the Y system variance. $\tilde{\sigma}^2_{\tilde{\mu}_y}$ conveys the uncertainty of the mean estimator.

2.3.2 General Variance Estimator

For the variance estimator stemming from Equation (7), one can use the χ^2 formulation in Appendix B to compute a generalized variance estimator for any given UT weights and sigma points. Noting that the distribution of the mean estimator is given in Equation (10), one can derive the distribution of the variance estimator by substituting the sigma point distributions into (7) as[1]

$$\sum_{i=0}^{N} \frac{w_i^c}{s_i^2} \left(\mathcal{N}\left(\mu_{y_i}, \sigma^2_{y_i}\right) - \mathcal{N}\left(\tilde{\mu}_y, \tilde{\sigma}^2_{\tilde{\mu}_y}\right)\right)^2 \sim \sum_{i=0}^{N} \frac{w_i^c}{s_i^2} \left(\mathcal{N}\left(\mu_{y_i} - \tilde{\mu}_y, \sigma^2_{y_i} + \tilde{\sigma}^2_{\tilde{\mu}_y}\right)\right)^2 \tag{13}$$

$$\sim \tilde{\chi}^2 \left(\begin{bmatrix} \frac{w_0^c}{s_0^2}\left(\sigma^2_{y_0} + \tilde{\sigma}^2_{\tilde{\mu}_y}\right) \\ \frac{w_1^c}{s_1^2}\left(\sigma^2_{y_1} + \tilde{\sigma}^2_{\tilde{\mu}_y}\right) \\ \vdots \\ \frac{w_N^c}{s_N^2}\left(\sigma^2_{y_N} + \tilde{\sigma}^2_{\tilde{\mu}_y}\right) \end{bmatrix}, \begin{bmatrix} 1 \\ 1 \\ \vdots \\ 1 \end{bmatrix}, \begin{bmatrix} \frac{\left(\mu_{y_0} - \tilde{\mu}_y\right)^2}{\sigma^2_{y_0} + \tilde{\sigma}^2_{\tilde{\mu}_y}} \\ \frac{\left(\mu_{y_1} - \tilde{\mu}_y\right)^2}{\sigma^2_{y_1} + \tilde{\sigma}^2_{\tilde{\mu}_y}} \\ \vdots \\ \frac{\left(\mu_{y_N} - \tilde{\mu}_y\right)^2}{\sigma^2_{y_N} + \tilde{\sigma}^2_{\tilde{\mu}_y}} \end{bmatrix} \right) \tag{14}$$

[1]It is noted that (13) assumes that (10) is distributed independently of y_i, which is incongruent since (10) is dependent on y_i. As such, the variance terms of (13) and the resultant overall distribution may be considered as upper bounds.

With this and equations (45) and (46), which denote the mean and variance, respectively, of a generalized χ^2 distribution, the above generalized variance estimator distribution has mean and variance as

$$\tilde{\sigma}_y^2 = \sum_{i=0}^{N} \frac{w_i^c}{s_i^2} \left(\sigma_{y_i}^2 + \tilde{\sigma}_{\tilde{\mu}_y}^2 + (\mu_{y_i} - \tilde{\mu}_y)^2 \right) \tag{15}$$

$$\sigma_{\sigma_y^2}^2 = 2 \sum_{i=0}^{N} \left(\frac{w_i^c}{s_i^2} \right)^2 \left(\left(\sigma_{y_i}^2 + \tilde{\sigma}_{\tilde{\mu}_y}^2 \right)^2 + 2 \left(\sigma_{y_i}^2 + \tilde{\sigma}_{\tilde{\mu}_y}^2 \right) (\mu_{y_i} - \tilde{\mu}_y)^2 \right) \tag{16}$$

It is true that (16) illustrates the uncertainty variance of the variance estimator. With this, we have knowledge of the confidence in the estimation of the variance. For the purposes of our work, this term is not immediately relevant, but we include it because of its equivalent derivation from the generalized χ^2 distribution and potential inclusion in future work.

2.3.3 Stochastic Unscented Transformation with Common Symmetric $N = 2$ Sigma Points

Recall from section 2.2.1, the two sigma points defined as $s_0 = +1$ and $s_1 = -1$ with weights as $w_0^a = w_1^a = w_0^c = w_1^c = \frac{1}{2}$. Inserting these values into the generalized mean and variance estimators yields

$$\tilde{\mu}_y = \frac{1}{2} \left(\mu_{y_0} + \mu_{y_1} \right) \tag{17}$$

$$\tilde{\sigma}_{\tilde{\mu}_y}^2 = \frac{1}{4} \left(\sigma_{y_0}^2 + \sigma_{y_1}^2 \right) \tag{18}$$

$$\tilde{\sigma}_y^2 = \frac{1}{2} \left(\sigma_{y_0}^2 + \sigma_{y_1}^2 + 2\tilde{\sigma}_{\tilde{\mu}_y}^2 + \left(\mu_{y_0} - \tilde{\mu}_y \right)^2 + \left(\mu_{y_1} - \tilde{\mu}_y \right)^2 \right) \tag{19}$$

$$= \frac{1}{2} \left(\sigma_{y_0}^2 + \sigma_{y_1}^2 + 2\tilde{\sigma}_{\tilde{\mu}_y}^2 + \frac{1}{2} \left(\mu_{y_0} - \mu_{y_1} \right)^2 \right) \tag{20}$$

Intuitively, we can now see the inherent contribution of incorporating the model uncertainty with the use of the stochastic unscented transform. By grouping the terms of (20), we realize the output variance uncertainty consists of 3 parts:

- The model/transform uncertainty: $\frac{1}{2} \left(\sigma_{y_0}^2 + \sigma_{y_1}^2 \right)$
- The transformed input distribution uncertainty (matching eq (9)): $\frac{1}{4} \left(\mu_{y_0} - \mu_{y_1} \right)^2$
- The uncertainty of the mean estimation: $\tilde{\sigma}_{\tilde{\mu}_y}^2$

Incorporating and accounting for all three of these terms derives the complete stochastic system characterization.

3. SUT VALIDATION

In this section, simple examples of a linear and a nonlinear system are presented followed by the results for space weather application where we use the output of a model that provides the index of the solar radio flux $F_{10.7}$ with uncertainty and CHAMP-ML model with the SUT approach. Finally, an orbit propagation is implemented using MSIS along with the inclusion of the $F_{10.7}$ with its uncertainty.

3.1 Linear System Example

Without loss of generality, any linear function, $y = f(x)$, can be simplified to the following diagram shown in Figure 2. Input values x are selected as members of an input normal distribution, X, the linear function f scales the input values by an arbitrary, deterministic scalar value, a, and then adds a random value b selected from a non-centric normal distribution, B, to produce $y = ax + b$. Here, the model also reports the variance of B (which is σ_b^2) as a secondary output, which is the uncertainty of the reported y value. Since the result is a simple Gaussian scale followed by a Gaussian addition, the true output distribution Y is Gaussian, where $\mu_y = a\mu_x + \mu_b$ and $\sigma_y^2 = a^2\sigma_x^2 + \sigma_b^2$.

With the given setup, the aim is to derive unscented symmetric estimator for accurately calculating the mean and variance for the given linear system in the example.

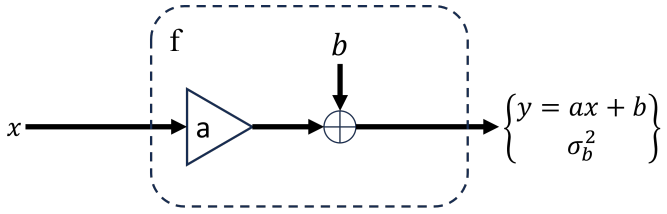

$$x \in X \sim \mathcal{N}(\mu_x, \sigma_x^2) \qquad b \in B \sim \mathcal{N}(\mu_b, \sigma_b^2) \qquad y \in Y \sim \mathcal{N}(\mu_y, \sigma_y^2)$$
$$\mu_y = a\mu_x + \mu_b$$
$$\sigma_y^2 = a^2\sigma_x^2 + \sigma_b^2$$

Fig. 3: Simple Linear System Example.

3.2 Unscented Symmetric N=2 Estimators

Using the results from Section 2.3.3, we can test the weighted mean and variance estimators. As specified by the symmetric $N = 2$ approach, the unscented mean and variance weights are all equal to $\frac{1}{2}$, and the input values are selected as $x_0 = \mu_x + \sigma_x$, $x_1 = \mu_x - \sigma_x$. With this,

$$y_0 = f(x_0) = f(\mu_x + \sigma_x) \sim \mathcal{N}\left(a(\mu_x + \sigma_x) + \mu_b, \sigma_b^2\right) \tag{21}$$
$$y_1 = f(x_1) = f(\mu_x - \sigma_x) \sim \mathcal{N}\left(a(\mu_x - \sigma_x) + \mu_b, \sigma_b^2\right) \tag{22}$$

representing the information outputted by the functional model.

Examining the expected value of the mean estimator, by using (17), yields

$$\tilde{\mu}_y = \frac{1}{2}\left(a(\mu_x + \sigma_x) + \mu_b + a(\mu_x - \sigma_x) + \mu_b\right) \tag{23}$$
$$= a\mu_x + \mu_b \tag{24}$$

displaying the correct (true) μ_y, validating the mean estimator for the symmetric $N = 2$ case.

For the variance estimator, we reference the generalized variance estimator (20) while also noting the variance of the mean estimator (18) and substitute our example values to yield

$$\tilde{\sigma}_y^2 = \frac{1}{2}\left(\sigma_{y_0}^2 + \sigma_{y_1}^2 + 2\tilde{\sigma}_{\tilde{\mu}_y}^2 + \frac{1}{2}\left(\mu_{y_0} - \mu_{y_1}\right)^2\right) \tag{25}$$
$$= \frac{3}{4}\sigma_{y_0}^2 + \frac{3}{4}\sigma_{y_1}^2 + \frac{1}{4}\left(\mu_{y_0} - \mu_{y_1}\right)^2 \tag{26}$$
$$= \frac{3}{2}\sigma_b^2 + a^2\sigma_x^2 \tag{27}$$

which, interestingly, fails to properly match the true variance estimate, as the σ_b^2 portion is $\frac{3}{2}$ of the intended amount. So, this estimator develops accurate capture of uncertainty contributions from the input but not from the model.

However, the findings in our studies show that the estimator is capable of matching accurately with the true output by establishing absolute confidence in the mean (i.e. $\tilde{\sigma}_{\tilde{\mu}_y} = 0$). Applying this idea we obtain

$$\tilde{\sigma}_y^2 = \frac{1}{2}\left(\sigma_{y_0}^2 + \sigma_{y_1}^2 + \frac{1}{2}\left(\mu_{y_0} - \mu_{y_1}\right)^2\right) \tag{28}$$
$$= \sigma_b^2 + a^2\sigma_x^2 \tag{29}$$

such that the correct unbiased variance estimator is derived. We arrive at the conclusion of the correct estimation by establishing the mean of variance estimator being equal to zero. Details of why this condition happens are explained in the end of this section.

3.3 Non Linear System Example

The conditions of this system are exactly the same as the Linear system, but with the new application of squaring the input of the model to implement the non-linearity aspect as displayed in the Figure below,

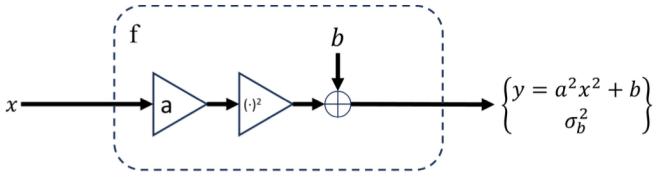

$x \in X \sim \mathcal{N}(\mu_x, \sigma_x^2)$ $\quad b \in B \sim \mathcal{N}(\mu_b, \sigma_b^2)$ $\quad y \in Y \sim \mathcal{N}(\mu_y, \sigma_y^2)$

$$\mu_y = a^2(\mu_x^2 + \sigma_x^2) + \mu_b$$

$$\sigma_y^2 = 2a^4\sigma_x^2(2\mu_x^2 + \sigma_x^2) + \sigma_b^2$$

Fig. 4: Simple Non-Linear System Example.

Again, we analytically test the weighted mean and variance estimators. Just like before,

$$y_0 = f(x_0) = f(\mu_x + \sigma_x) \sim \mathcal{N}\left(a^2(\mu_x + \sigma_x)^2 + \mu_b, \sigma_b^2\right) \tag{30}$$

$$y_1 = f(x_1) = f(\mu_x - \sigma_x) \sim \mathcal{N}\left(a^2(\mu_x - \sigma_x)^2 + \mu_b, \sigma_b^2\right) \tag{31}$$

We go ahead and examine the expected value using (17) and the mean estimation yields,

$$\tilde{\mu}_y = \frac{1}{2}\left(a^2(\mu_x + \sigma_x)^2 + \mu_b + a^2(\mu_x - \sigma_x)^2 + \mu_b\right) \tag{32}$$

$$= a(\mu_x^2 + \sigma_x^2) + \mu_b \tag{33}$$

Thus, displaying an accurate capture of the mean for the nonlinear case. The symmetric case for mean estimation is validated.

Proceeding with the variance estimation, we note that the variance of the mean estimator, using (18), gives

$$\tilde{\sigma}_{\tilde{\mu}_y}^2 = \frac{1}{4}(\sigma_b^2 + \sigma_b^2) = \frac{1}{2}\sigma_b^2 \tag{34}$$

Then, we proceed to use the generalized variance estimator (18) and substitute our values,

$$\tilde{\sigma}_y^2 = \frac{1}{2}\left(\sigma_{y_0}^2 + \sigma_{y_1}^2 + 2\tilde{\sigma}_{\tilde{\mu}_y}^2 + \frac{1}{2}\left(\mu_{y_0} - \mu_{y_1}\right)^2\right) \tag{35}$$

$$= \frac{3}{2}\sigma_b^2 + 4a^4\mu_x^2\sigma_x^2 \tag{36}$$

We observe similar behavior as the linear system where and overestimation of 3/2 of the uncertainty being reported from the model and again, the σ_x^4 term is missing. From the result, applying absolute confidence in the mean estimator will yield the correct variance reported from the model and if we also insert the missing higher-order term $2a^4\sigma_x^4$. With this, we get

$$\tilde{\sigma}_y^2 = \sigma_b^2 + 4a^4\mu_x^2\sigma_x^2 + 2a^4\sigma_x^4, \tag{37}$$

which now provides the correct estimation for the variance estimator. This result implies that for the conditions to obtain correct estimation, a correction factor needs to be implemented and that factor will depend on the nature of the non-linearity of the model itself, and of course, assume perfect confidence in the mean estimation.

3.4 Space Weather Application

In this section, we analyze the overall output of stochastic density model driven by an input distribution (mean and variance) of the space weather index. Two different scenarios consisting of a low solar activity and high solar activity for the solar radio flux as defined in previous work [19] are used. We apply the generalized estimators for the mean and variance estimation. The model selected for this study was CHAMP-ML. The $F_{10.7}$ distribution is obtained using the models developed in [11]. We proceed to use the rules of UT to establish the input points. The model reports neutral atmospheric density with a source of uncertainty where we can implement the SUT method. We establish a Monte Carlo simulation as our ground truth. The parameters for each scenario are shown in Table 1. The scenarios are shown below,

Table 1: Space Weather Parameters for each scenario

	Mean Solar Flux (F10.7)	Variance	Case
Scenario 1	73.6 sfu	54.8	Low Solar Activity
Scenario 2	224.7 sfu	175.6	High Solar Activity

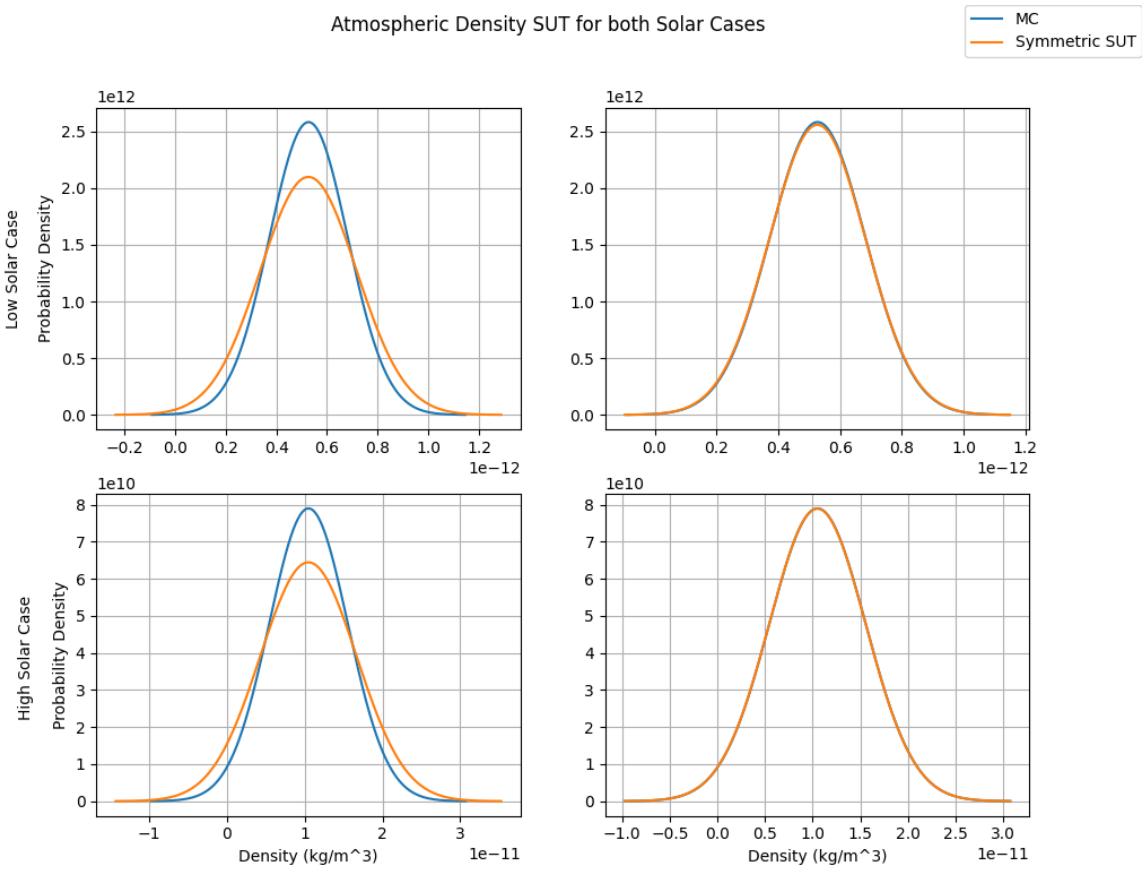

Fig. 5: Output results from CHAMP-ML with SUT approach. Leftmost panels display results of the general estimators including the variance of the mean estimator. Rightmost panels displays the results of the general estimators without the inclusion of the variance of the mean estimator

From Figure 5, we have two illustrations: rightmost panels contains the results from Equations (17) and (20) for the common symmetric case, whereas, the leftmost panels show the General Estimators where the Variance of the Mean Estimator $\tilde{\sigma}_{\mu}^{2} \neq 0$. There is an overestimation bias in the leftmost panels for the symmetric case, respectively, making it unable to report the correct output. For the rightmost panels, the same results happen here as for the basic linear

example shown previously. The results in the leftmost panels matches accurately the expected overestimation of 3/2 due to the inclusion of the variance from the mean estimator.

From all the examples, we observe an equivalent behaviour of the estimators. An overestimation of the uncertainty from the model is being reported as we apply the variance of the mean estimator. When we set the variance of the mean estimator to zero, we capture the correct distribution matching the output from all example cases. In the nonlinear case, we must not forget an additional correction factor is needed for correct capture of the variance besides the correction factor for σ_b^2. The SUT approach tends to overestimate the variance of the mean, inflating the variance of the model in the output by 1/2 for all the cases. For the CHAMP-ML case, we observe in the different solar cases, the response of the model captures closely the nature of $F_{10.7}$ linearly.

4. SUT FOR ORBIT AND UNCERTAINTY PROPAGATION

4.1 SUT and Simulation Scenario Setup

After applying the generalized SUT framework for obtaining the joint statistics on density resulting from both driver and model uncertainty, we employ SUT for orbit and uncertainty propagation. The case of 2-tier SUT application for end-to-end processing is schematically represented in Figure 6. To isolate the effects on density and drag uncertainty, we set the initial state covariance to a small value. The current SUT framework supports 1-dimensional application. Therefore, we consider the uncertainty in the $F_{10.7}$ space weather driver obtained from the model of [11]. We use the MSIS00 model for density apply a constant level of model uncertainty. While we have several probabilistic models available, we chose MSIS00 because the HASDM-ML and CHAMP-ML use other solar drivers that require a n-dimensional SUT to accurately account for uncertainty. They can be used with future extensions of the SUT framework. The initial version of the TIE-GCM ROPE model is limited to an altitude of 450 km. Extension of the model to higher LEO altitude is currently underway.

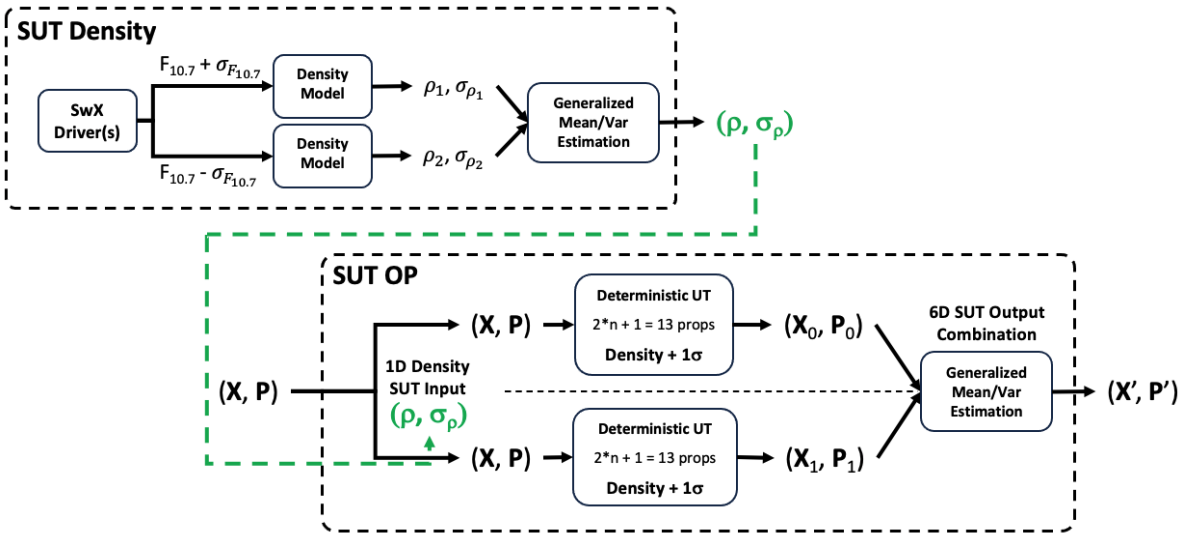

Fig. 6: A schematic of the application of SUT for density uncertainty estimation and state and covariance propagation.

The simulation parameters are summarized in Table 2. We simulate the strongest storm over the last 30 years, the Halloween storm of 2003, to highlight the impact of drag and uncertainties on operations. Figure 7 shows the density during the three day storm period as well as the drivers. The Halloween storm has two days of strong storm activity resulting from two stacked coronal mass ejections (CMEs).

4.2 State and Uncertainty Propagation Results

Figure 8 shows the results of the density uncertainty characterization with SUT and its impact on covariance propagation. As previously mentioned, the $F_{10.7}$ mean and uncertainty forecasts are derived from the models of [11]. Different levels of model uncertainty are implemented around the mean density from MSIS00 ranging from 5-30%. It

Table 2: Simulation set-up for the orbit uncertainty propagation using SUT and MC approach.

Parameter	Value/Details
Initial position (ECI)	[3782900.7032, -5441600.6779, -1420075.1327] m
Initial velocity (ECI)	[-606.6600, 1539.2559, -7488.3946] m/s
State	Position and Velocity
Dynamic Model	2-body, J2 and drag
Propagation period	3 days
Object shape/type	Spherical & symmetric
Cross-sectional AMR	0.002 m^2/kg
Drag coefficient	2.2
Initial epoch	00:00:00 UTC, October 29, 2003 - Halloween Storm
Orbit propagation method	SUT Modified MC 2 (Paul et. al.) half-life = 18 min, 180 min, and ∞
Number of MC iterations	1000

is observed that while the impact of driver uncertainty remains constant, the overall position deviation is significantly influenced by changes in model uncertainty. As model uncertainty increases, the position uncertainty also increases.

The stochastic models (e.g. HASDM-ML) suggest that the model uncertainty level during a storm period like the Halloween storm is expected to be between 25-30%. Therefore, position uncertainty of tens of kilometers in operations can be expected after 3 days of propagation. It is important to note that the driver uncertainty currently does not include the uncertainty in storm-time driver, A_p. We expect that with uncertainty in A_p considered, the contribution of the space weather drivers to position uncertainty will be significantly larger. Even during non-storm conditions, at the level of 5-10% model uncertainty, position uncertainty of several kilometers can be expected after a 3-day propagation during high solar activity at approximately 400 km altitude.

As a reminder to the reader, these position deviations are for the scenario where orbit is propagated without any new observations and are most suitable for conjunction assessments. The ground tracking of a resident space object

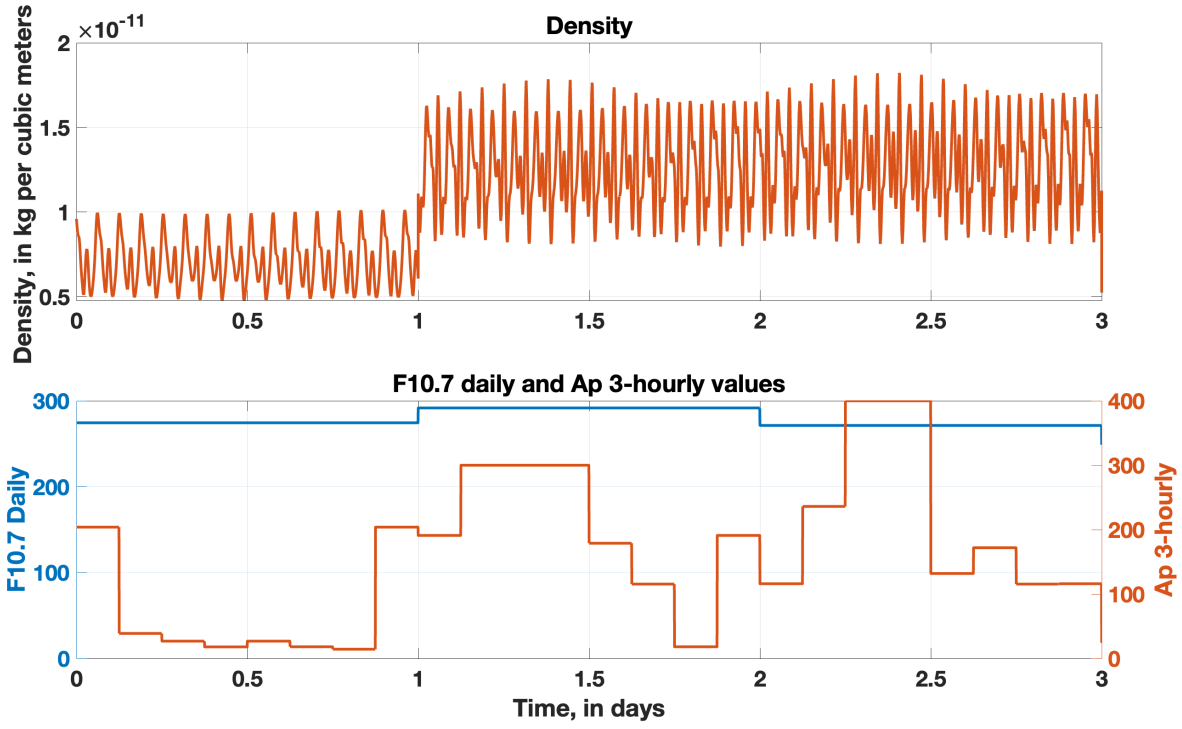

Fig. 7: Density and driver values from the NRLMSISE-00 atmospheric density model during the Halloween 2003 storm. Epoch is from the 29th October to 1st November 2003.

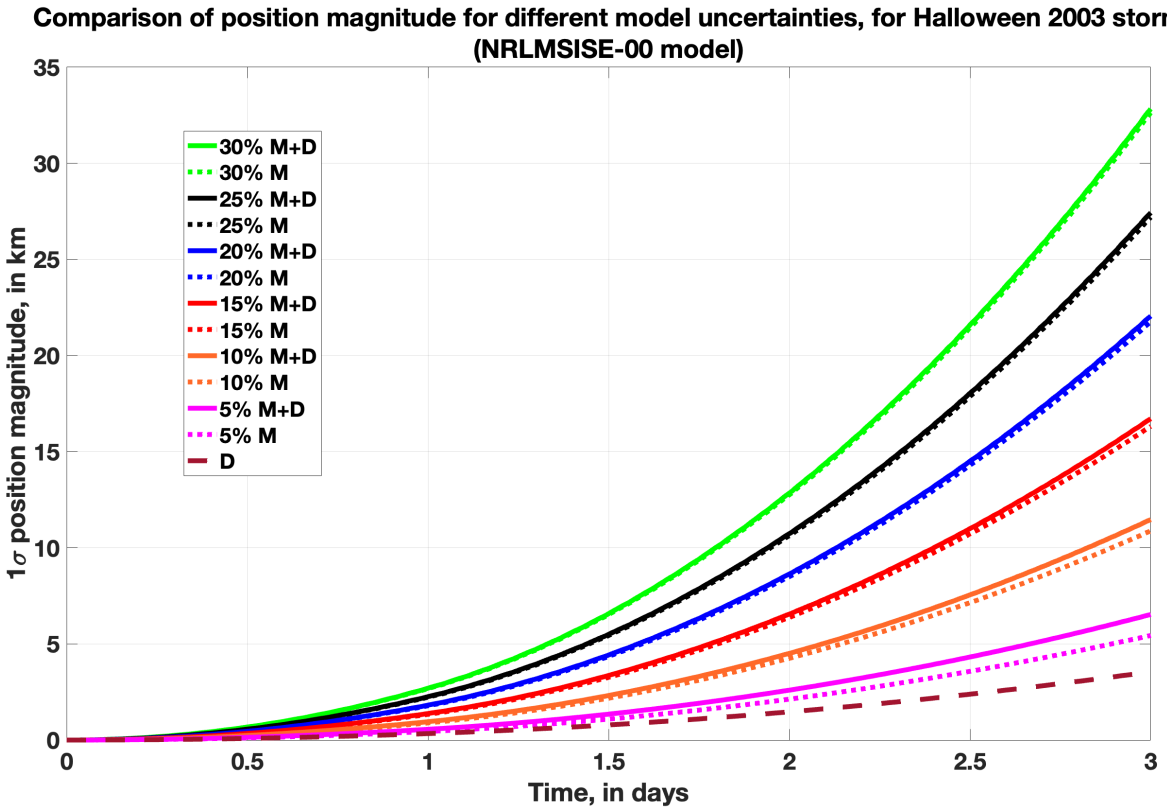

Fig. 8: Propagated position deviation for a LEO orbit. Different model (M) and driver (D) uncertainty combinations have been simulated for high solar activity conditions using the NRLMSISE-00 atmospheric density model. Epoch is from the 29th October to 1st November 2003 at a timestep of 10 seconds.

(RSO) relies on various parameters, these include orbital characteristics (including altitude, eccentricity, and inclination), object properties (including dimensions, shape, surface reflectivity, and maneuverability), sensor characteristics (including telescope aperture size, resolution, sensitivity, and radar frequency), and environmental factors (including atmospheric conditions, cloud cover, and solar phase angle). Typically, majority of cataloged objects at the LEO altitude have an average revisit rate of 1-2 observations per day, while median revisit rate is generally around 3-4 observations per day. The operational RSOs are some of the most well-tracked objects and can have up to 7-8 observations each day [20]. However, during the storm conditions or when objects maneuver, ground tracking is disrupted which can significantly affect the revisit rates to an extent that some RSOs can go missing for days. The purpose of presenting the results for propagation-only scenario is to simulate the ”worst-case” tracking performance during adverse conditions. The objective is to assess the overall trajectory deviation, thereby showcasing the capabilities of proposed approach to realistically model uncertainties without additional tracking data.

4.3 Monte Carlo Validation

We employ a Monte Carlo (MC) algorithm to validate the orbit and uncertainty propagation algorithm using SUT. We follow the methods of Paul et. al., to implement the MC algorithm to account for the uncertainty in density [21]. We use the same initial conditions as in the SUT framework and simulate three cases with different half-lives for a first order Gauss-Markov process to model atmospheric density uncertainty. The Gauss-Markov process models the temporal autocorrelation of atmospheric density fluctuations compared to simpler models. This approach allows for a more realistic simulation of the stochastic nature of atmospheric drag, a critical factor in orbit propagation at LEO altitudes. The MC simulation parameters including the half-lives considered are also given in Table 2.

Residuals are calculated as the absolute position error for each MC run with respect to the mean trajectory. The results demonstrated a notable spread in the spacecraft’s position, with deviations growing over the 3-day propagation period. This spread is more pronounced in the along-track direction, reflecting the cumulative effect of atmospheric drag acting

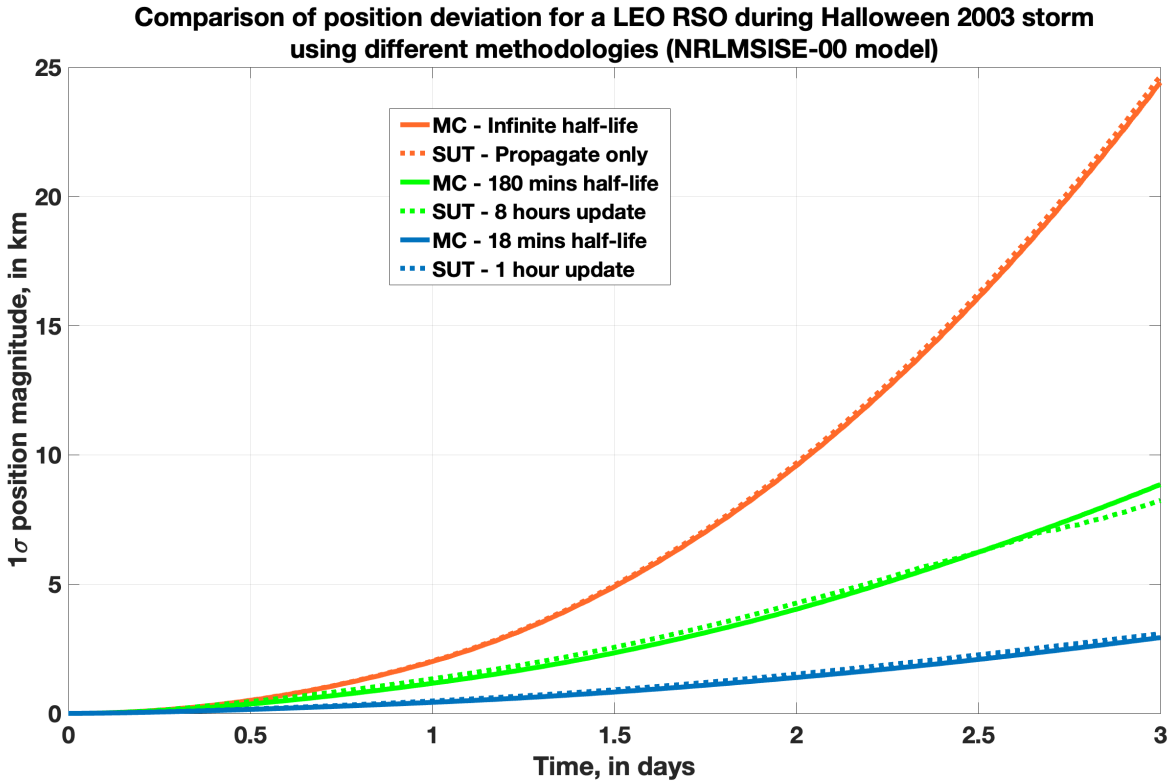

Fig. 9: Propagated position deviation for a LEO orbit using Monte Carlo and SUT. Results have been simulated for the Halloween storm conditions using the NRLMSISE-00 atmospheric density model. Epoch is from the 29th October to 1st November 2003 at a timestep of 10 seconds. Three cases are presented for Monte Carlo with different half-life for the atmospheric density uncertainty, whereas for SUT different update times matching with corresponding Monte Carlo results have been shown.

over time. A key observation from the results was the relationship between the half-life of the Gauss-Markov process and the position deviation. As the half-life increases, decay of density perturbations decreases, thereby increasing the position deviation as the long-lasting atmospheric density variations are consistently applied on the spacecraft's trajectory, leading to greater uncertainty in position.

Figure 9 confirms this trend, showing larger deviations from the mean trajectory as the half-life increased. Overall, the findings underscore the importance of accounting for the temporal characteristics of atmospheric density when modeling drag forces in LEO. The challenge is to identify what half-life represents the truth. This can only be achieved through comparison with measurements and will be a subject of future work for us. Figure 9 also shows the comparison of the SUT propagated position uncertainty with that from the MC simulations. By default since the SUT framework tracks the +/- 1σ uncertainty in density, it represent a half-life of ∞ as simulated with MC. Simulating non infinity MC half-lives with SUT requires manual tuning how often the sigma points get orthogonalized. As shown in Figure 9, for a 180 min half-life, a orthogonalization time of 8 hours in required while for a half-life of 18 min, a orthogonalization time of 1 hour is required.

5. CONCLUDING DISCUSSION AND FUTURE WORK

Accurately modeling of the dynamic space environment and effective incorporation of said variations into orbital dynamics of space objects through drag modeling is a critical challenge that requires innovative solutions. Existing operations use models that carry two primary limitations: limited-fidelity and deterministic. Improving the fidelity and developing probabilistic capabilities are essential to achieving advances in orbit determination and prediction.

We are developing the next-generation drag modeling which will integrate several technical innovations. The first

innovative element was recently established in the form of stochastic/probabilistic models for neutral mass density. The second innovation is the development of state-of-the-art probabilistic models for the drivers of the density models. We have developed models for the solar driver(s) ($F_{10.7}$) while several community efforts have been dedicated for the geomagnetic driver (A_p).

This works presents the next in line of innovation, a mathematical framework we call stochastic unscented transform (SUT) that efficiently and effectively provides the joint statistics resulting from probabilistic input models ($F_{10.7}$ and A_p) driving stochastic neutral density models. We present the mathematical derivation of the SUT framework as well as its validation with simple linear and nonlinear examples and finally a space weather example. Because the SUT framework is highly general in nature, we also demonstrate its application to the case of orbit covariance propagation. We successfully validate the covariance propagation with Monte Carlo simulations.

The close agreement between the SUT and MC results confirms the validity of the SUT framework in modeling the complex interactions between atmospheric density and spacecraft dynamics in LEO. Incorporation of this in the orbital propagation is novel as the stochastic trends are translated to orbital dynamics in real-time thereby reducing the latency. This methodology is particularly valuable for day-to-day space operations, as it facilitates covariance realism and enhanced conjunction assessment. In a conjunction assessment, atmospheric density is typically assumed to be constant and the corresponding stochastic behavior is generally not incorporated while calculating the probability of collision (Pc). These assumptions can fail during the high solar activity and storm scenarios where the atmospheric drag perturbation can significantly impact the relative trajectories of the two RSOs. Realistic conjunction assessment can significantly influence Go/No-Go decision for satellite operators and is particularly important during high risk conjunctions [22]. The SUT framework proposed in this work helps in incorporating the drag uncertainties in the propagated orbit of each RSO which consequently help improve conjunction assessment and Pc calculation.

Current limitations of the SUT framework include 1-dimensional and Gaussian distribution assumption. Future work will focus on extending the SUT framework for n-dimensional and multi-variations. Further extension will attempt to capture non-Gaussian statistics.

ACKNOWLEDGEMENTS

This research is based upon work support in part by the Office of the Director of National Intelligence (ODNI), Intelligence Advance Research Projects Activity (IARPA), via 2023-23060200005. The views and conclusions contained herein are those of the authors and should not be interpreted as necessarily representing official policies, either expressed or implied, of ODNI, IARPA, or the U.S. Government. The U.S. Government is authorized to reproduce and distribute reprints for governmental purposes notwithstanding any copyright annotation therein'.

6. APPENDICES

APPENDIX A - COMMON LINEAR GAUSSIAN OPERATIONS

Common Gaussian linear transformations are noted here. For these, let $X \sim \mathcal{N}\left(\mu_x, \sigma_x^2\right)$ and $Y \sim \mathcal{N}\left(\mu_y, \sigma_y^2\right)$, where X and Y are independently distributed.

Translation:
Let a be a deterministic scalar, then

$$X \pm a \sim \mathcal{N}\left(\mu_x \pm a, \sigma_x^2\right) \tag{38}$$

Scaling:

$$aX \sim \mathcal{N}\left(a\mu_x, a^2\sigma_x^2\right) \tag{39}$$

Addition:
Let b be another deterministic scalar, then

$$X \pm Y \sim \mathcal{N}\left(\mu_x \pm \mu_y, \sigma_x^2 + \sigma_y^2\right) \tag{40}$$

$$aX \pm bY \sim \mathcal{N}\left(a\mu_x \pm b\mu_y, a^2\sigma_x^2 + b^2\sigma_y^2\right) \tag{41}$$

APPENDIX B - GENERALIZED GAUSSIAN SQUARES

Let $X \sim \mathcal{N}\left(\mu, \sigma^2\right)$ and a be a deterministic scalar, then $aX^2 \sim \tilde{\chi}^2\left(a\sigma^2, 1, \frac{\mu^2}{\sigma^2}\right)$, where $\tilde{\chi}^2$ denotes a generalized χ^2 distribution [23]. This can be shown by first noting that

$$\frac{X}{\sigma} \sim \mathcal{N}(\mu, 1). \tag{42}$$

From here, with a normalized (unit-variance) Gaussian, we can square this result to formulate a non-central χ^2 distribution [24] as

$$\left(\frac{X}{\sigma}\right)^2 = \frac{X^2}{\sigma^2} \sim \chi_1^2\left(\frac{\mu^2}{\sigma^2}\right), \tag{43}$$

noting the χ^2 distribution's degree-of-freedom ($k = 1$), and non-centrality parameter ($\lambda = \frac{\mu^2}{\sigma^2}$).
With this, we can now multiply by the desired scalar, a, and reapply the proper variance, by noting that

$$aX^2 = a\sigma^2\left(\frac{X^2}{\sigma^2}\right) \sim \tilde{\chi}^2\left(a\sigma^2, 1, \frac{\mu^2}{\sigma^2}\right), \tag{44}$$

where the generalized χ^2 distribution's scaling parameter ($\mathrm{w} = a\sigma^2$), degree-of-freedom ($\mathrm{k} = 1$), and non-centrality parameter ($\lambda = \frac{\mu^2}{\sigma^2}$).

Of particular interest, it can be noted [23] that the generalized χ^2 distribution notated as $\tilde{\chi}^2(\mathrm{w}, \mathrm{k}, \lambda)$ has a mean of

$$\sum_j \mathrm{w}_j\left(\mathrm{k}_j + \lambda_j\right) \tag{45}$$

and variance of

$$2\sum_j \mathrm{w}_j^2\left(\mathrm{k}_j + 2\lambda_j\right). \tag{46}$$

Thus for (44), the resultant mean is

$$a\left(\mu^2+\sigma^2\right) \tag{47}$$

with variance

$$2a^2\sigma^2\left(2\mu^2+\sigma^2\right) \tag{48}$$

Note: Multiple Gaussian squares can be additively combined by vectorizing the w, k, and λ parameters as

$$aX^2+bY^2 \sim \tilde{\chi}^2\left(\begin{bmatrix}a\sigma_x^2\\ b\sigma_y^2\end{bmatrix}, \begin{bmatrix}1\\1\end{bmatrix}, \begin{bmatrix}\frac{\mu_x^2}{\sigma_x^2}\\ \frac{\mu_y^2}{\sigma_y^2}\end{bmatrix}\right) \tag{49}$$

Lastly, if an additional, independent Gaussian Random Variable, $\mathcal{B} \sim \mathcal{N}(\mu_b, \sigma_b^2)$, is added, then one can make use of the (optional) additional parameters associated with the generalized χ^2 distribution. With these, it may be shown that

$$aX^2+B \quad \sim \quad \tilde{\chi}^2\left(a\sigma^2, 1, \frac{\mu^2}{\sigma^2}, \sigma_b, \mu_b\right), \tag{50}$$

where the system mean can be analytically expressed as

$$a\left(\mu^2+\sigma^2\right)+\mu_b \tag{51}$$

and the system variance is

$$2a^2\sigma^2\left(2\mu^2+\sigma^2\right)+\sigma_b^2. \tag{52}$$

REFERENCES

[1] Richard J. Licata and Piyush M. Mehta. Uncertainty quantification techniques for space weather modeling: Thermospheric density application. *CoRR*, abs/2201.02067, 2022.

[2] Nathan Stacey and Simone D'Amico. Analytical process noise covariance modeling for absolute and relative orbits. *Acta Astronautica*, 194:34–47, 2022.

[3] Mark F. Storz, Bruce R. Bowman, Major James I. Branson, Stephen J. Casali, and W. Kent Tobiska. High accuracy satellite drag model (hasdm). *Advances in Space Research*, 36(12):2497–2505, 2005. Space Weather.

[4] L. Newman, R. Besser, and M. Hejduk. Predicting Space Weather Effects on Close Approach Events. In S. Ryan, editor, *Advanced Maui Optical and Space Surveillance Technologies Conference*, page 39, January 2015.

[5] Bruce Bowman and W. K. Tobiska. JB2008: Empirical Thermospheric Density Model. Astrophysics Source Code Library, record ascl:2007.021, July 2020.

[6] Piyush M. Mehta, Andrew Walker, Craig A. McLaughlin, and Josef Koller. Comparing physical drag coefficients computed using different gas–surface interaction models. *Journal of Spacecraft and Rockets*, 51(3):873–883, 2014.

[7] J. T. Emmert, D. P. Drob, J. M. Picone, D. E. Siskind, M. Jones Jr., M. G. Mlynczak, P. F. Bernath, X. Chu, E. Doornbos, B. Funke, L. P. Goncharenko, M. E. Hervig, M. J. Schwartz, P. E. Sheese, F. Vargas, B. P. Williams, and T. Yuan. Nrlmsis 2.0: A whole-atmosphere empirical model of temperature and neutral species densities. *Earth and Space Science*, 8(3):e2020EA001321. e2020EA001321 2020EA001321.

[8] Richard J. Licata, Piyush M. Mehta, W. Kent Tobiska, and S. Huzurbazar. Machine-Learned HASDM Thermospheric Mass Density Model With Uncertainty Quantification. *Space Weather*, 20(4), 2022.

[9] Richard J. Licata, Piyush M. Mehta, Daniel R. Weimer, W. Kent Tobiska, and Jean Yoshii. Msis-uq: Calibrated and enhanced nrlmsis 2.0 model with uncertainty quantification. *Space Weather*, 20(11):e2022SW003267, 2022. e2022SW003267 2022SW003267.

[10] Richard J. Licata and Piyush M. Mehta. Reduced order probabilistic emulation for physics-based thermosphere models. *Space Weather*, 21(5), May 2023.

[11] Joshua D. Daniell and Piyush M. Mehta. Probabilistic solar proxy forecasting with neural network ensembles. *Space Weather*, 21(9):e2023SW003675, 2023. e2023SW003675 2023SW003675.

[12] Joshua D. Daniell and Piyush M. Mehta. Probabilistic short-term solar driver forecasting with neural network ensembles. *Space Weather*, 22(3):e2023SW003785, 2024. e2023SW003785 2023SW003785.
[13] Evangelos Paouris, Maria Abunina, Anatoly Belov, and Helen Mavromichalaki. Statistical analysis on the current capability to predict the ap geomagnetic index. *New Astronomy*, 86:101570, 2021.
[14] Chakraborty, Shibaji and Morley, Steven Karl. Probabilistic prediction of geomagnetic storms and the kp index. *J. Space Weather Space Clim.*, 10:36, 2020.
[15] S.J. Julier and J.K. Uhlmann. Unscented filtering and nonlinear estimation. *Proceedings of the IEEE*, 92(3):401–422, 2004.
[16] Donald Ebeigbe, Tyrus Berry, Michael M. Norton, Andrew J. Whalen, Dan Simon, Timothy Sauer, and Steven J. Schiff. A generalized unscented transformation for probability distributions, 2021.
[17] Simon J. Julier and Jeffrey K. Uhlmann. New extension of the kalman filter to nonlinear systems. In *Defense, Security, and Sensing*, 1997.
[18] E.A. Wan and R. Van Der Merwe. The unscented kalman filter for nonlinear estimation. In *Proceedings of the IEEE 2000 Adaptive Systems for Signal Processing, Communications, and Control Symposium (Cat. No.00EX373)*, pages 153–158, 2000.
[19] Richard J. Licata, W. Kent Tobiska, and Piyush M. Mehta. Benchmarking forecasting models for space weather drivers. *Space Weather*, 18(10):e2020SW002496, 2020. e2020SW002496 10.1029/2020SW002496.
[20] Darren McKnight, Rachit Bhatia, Erin Dale, Chris Gates, Owen Marshall, Adam Marsh, and Mohin Patel. Analytic space domain awareness. In *Proceedings of the Advanced Maui Optical and Space Surveillance (AMOS) Technologies Conference*, September 2023.
[21] Smriti Nandan Paul, Richard J Licata, and Piyush M Mehta. Advanced ensemble modeling method for space object state prediction accounting for uncertainty in atmospheric density. *Advances in Space Research*, 71(6):2535–2549, 2023.
[22] Rachit Bhatia and Darren McKnight. Assessment of evolving conjunction risk for small satellite missions. In *Small Satellite Conference*, 2023.
[23] DA Jones. Statistical analysis of empirical models fitted by optimization. *Biometrika*, 70(1):67–88, 1983.
[24] PB Patnaik. The non-central χ 2-and f-distribution and their applications. *Biometrika*, 36(1/2):202–232, 1949.